Modeling Propagation of Seismic Airgun Sounds and the Effects on Fish Behavior

Jens M. Hovem, *Member, IEEE*, Tron Vedul Tronstad, Hans Erik Karlsen, and Svein Løkkeborg

***Abstract*—High activity of seismic surveying in Norwegian waters has caused concerns about the impact the acoustic noise from the seismic airguns may have on marine life. There is evidence that this noise can cause reactions on the behavior of the fish resulting in reduced catches. To mitigate the problem and the conflict of interest between the fishing industry and the seismic exploration interest, the Norwegian Petroleum Directorate (NPD) commissioned SINTEF Information and Communication Technology (ICT, Trondheim, Norway) and the Department of Biology, University of Oslo (Oslo, Norway) to develop an acoustic–biological model to predict the impact of seismic noise on the fish population. The ultimate goal is to develop an acoustic–biological model to use in the design and planning of seismic surveys such that the disturbance to fishing interest is minimized. This acoustic module of the model is based on ray theory and can deal with range-dependent bathymetry and depth-dependent sound-speed profiles. The bottom is modeled as a sedimentary fluid layer over a solid elastic rock and the model requires the thickness and seismoacoustic properties of the sediments layer and the rock with compressional speed, shear speed, and absorption. The model simulates the total sound field, both in the time domain and in the frequency domain, out to very large distances. Calculated sound exposure levels are compared with startle response levels for cod. Preliminary conclusions indicate a required distance in the range of 5–10 km, but dependent on the depth and the season. In additions, under certain conditions, there will appear regions with hot spots where the sound level is significantly higher due to caustics and focusing of sound. Modeled results are compared with results obtained from a joint seismoacoustic survey conducted in summer 2009 at Vesterålen-Lofoten area (Nordland VII). In this experiment, signals were recorded at fixed hydrophone positions as the seismic vessel approached from a maximum distance of 30 km toward the receiving positions. The same situation was modeled using available geological and oceanographic information as input to the acoustic model. The agreement between the real and recorded signals and the model results is good. This indicates that in the future acoustic–biological models may be used in the design and planning of seismic surveys such that the disturbance to fishing is minimized.**

***Index Terms*—Computer modeling, directivity, fish behavior, ray tracing, transmission loss (TL), underwater acoustic propagation.**

Manuscript received June 14, 2011; revised May 22, 2012; accepted June 18, 2012. Date of publication August 24, 2012; date of current version October 09, 2012.

Associate Editor: W. M. Carey.

J. M. Hovem is with the Department of Electronics and Telecommunication, The Norwegian University of Science and Technology (NTNU), Trondheim 7034, Norway and also with SINTEF Information and Communication Technology (ICT) Acoustics, Trondheim 7465, Norway (e-mail: hovem@iet.ntnu.no).

T. V. Tronstad is with SINTEF Information and Communication Technology (ICT) Acoustics, Trondheim 7465, Norway (e-mail: tronvedul.tronstad@sintef.no).

H. E. Karlsen is with the Drøbak Marine Biological Field Station, Institute of Biology, University of Oslo, Oslo 0316, Norway (e-mail: h.e.karlsen@bio.uio.no).

S. Løkkeborg is with the Institute of Marine Research, Bergen 5005, Norway (e-mail: svein.loekkeborg@imr.no).

Color versions of one or more of the figures in this paper are available online at http://ieeexplore.ieee.org.

Digital Object Identifier 10.1109/JOE.2012.2206189

I. Introduction

MARINE seismic exploration uses airguns or airgun arrays to generate high-energy, short-duration acoustic pulses into the subsea strata. These pulses are reflected back to receivers (hydrophones) in the water. By studying the structure of the received signal, the geophysicists draw conclusions about the structure beneath the seafloor. The construction and the configuration of airguns and arrays are optimized for transmission of seismic/acoustic energy downwards into the underground. However, some of the energy remains in the water column, undergoing multiple reflections at the bottom and sea surface. This acoustic energy is significant because the energy level of the source is high. Therefore, the airgun sound energy can propagate to considerable distances and cause disturbance to marine life, such as fish and marine mammals.

The sketch in Fig. 1 describes the situation and how the impulsive sound from an airgun source may propagate to long distances in the ocean. The source emits sound in all directions and some of these are indicated by arrows. Sound hitting the sea bed is partly transmitted into the bottom and partly reflected from the bottom. The interaction with the near sea bottom is described by a bottom reflection coefficient. Sound that strikes the bottom in the vertical direction experiences a relatively small reflection coefficient with most of the energy being transmitted into the bottom. Sound that hits the bottom with angles closer to the horizontal angle than the critical angle θ_{crit} will experience almost total reflection and consequently a very small loss. The critical angle is given by the ratio of the sound speeds in the sea water to the sound speed in the bottom, and will typically be around 20°. Sound striking the bottom at angles smaller than the critical angle may therefore propagate and be audible to fish and marine mammals at very long ranges.

Predicting the level of sound from a seismic source is difficult, and use is generally made of empirical models for its estimation. A simple and basic model that is often used relates the sound pressure level (SPL) to the source level (SL) diminished by the transmission loss (TL) by an equation of the form

$$\mathrm{SPL} = \mathrm{SL} - \mathrm{TL}. \tag{1}$$

The SL is dependent on the strength of the airguns and the directional properties of the array, i.e., the amplitudes and time structure of the transmitted signal in all directions; such information is normally not available.

The received sound at a given position is compared with a hearing threshold HL such that if SPL $>$ HL, it is judged that fish in the location may be affected by the received SPL. The judgment has to be made based on the three factors:

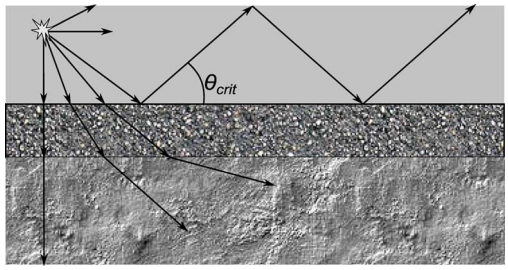

Fig. 1. A sketch indicating propagation of sound over a layered sea bed.

- SL including directionality;
- TL in the water including the effects of reflections from the sea surface and bottom;
- the respond threshold (RT) of the actual species of fish.

All three quantities are unknowns and even not strictly or uniquely defined. For instance, it is not clear what features of the received sound affect fish behavior. Is it the peak sound pressure, the mean or average pressure, or some other characteristic of the sound?

For the TL it has become customary [1] to express the loss with a simple empirical equation of the form

$$\mathrm{TL} = N \log_{10}(r) + \alpha r \tag{2}$$

where N is determined experimentally and α is the frequency-dependent absorption coefficient for acoustic waves in water. For the ranges and frequencies of interest to this study the last term in (2) is of minor importance and can be ignored.

We think that this expression for the TL described by (2) is much too simplistic. More reliable prediction of the sound propagation loss may be obtained by using modern propagation models. This is the issue discussed in this paper with examples of situations where the simple expression in (2) is wrong and misleading.

This paper describes an acoustic propagation model and its use to calculate the full waveform responses, in the time and frequency domain, from airguns to distance of up to 30 km. The modeled results are compared with recorded signals obtained in a joint seismic–acoustic survey in the Vesterålen area (Nordland VII) in summer 2009. The agreement between the real recorded signals and the model results is good. This indicates that in the future, acoustic–biological models may be used in the design and planning of seismic surveys such that the disturbance to fishing interest is minimized.

II. Modeling the Propagation of Sound in the Ocean

Modeling of acoustic propagation conditions has always been an important issue in underwater acoustics and there exist several mathematical/numerical models based on different methods; see [2] for an overview. The frequency range of interest for fish disturbance and annoyance is from 10 to 1000 Hz [3], [4]. Broadly speaking, this is also the frequency for passive sonar used by the navies to detect and monitor submarines by analyzing the radiated acoustic noise. However, airgun sounds are transient impulsive signal and not stationary noise sources. This means that a capability to model the time structure is necessary, which requires simultaneous modeling of many frequencies (approximately 1000) to compute the full waveform of the airgun signals.

After a preliminary study of available models and their capabilities it was concluded to use ray theory, but supplemented with a wave number integration model. A ray tracing program PlaneRay [5] was used in addition to a wave number integration model OASES [6]. The ray approach is known to have limited accuracy at very low frequencies (less than 25 Hz in the current application) and the effects of the bottom interaction are treated in an approximate manner. The OASES model has other practical limitations and can only handle range-independent situations (in the basic version) with no variations in water depth and bottom parameters with range. Because of its high accuracy we also use the OASES model to verify the results in situations where the application of ray theory may be suspect. The accuracy of the PlaneRay model has been tested extensively by comparing it with the OASES model for range-independent cases and was found to be sufficiently accurate for frequencies above 25 Hz for all the applications treated in this text [4], [7].

III. The Ray Trace Model

Fig. 2 shows the general propagation scenario that can be modeled with the PlaneRay model. The sound-speed profile in the water is limited to be a function of depth only and is not allowed to vary in the horizontal direction. Rays are only traced to the water–sediment interface and not into the bottom, and the acoustic effect of the bottom is represented by plane wave reflection coefficients. The bottom may be layered and, in principle, any number of fluid and elastic layers is allowed, but in the current version, only a fluid sedimentary layer over elastic half-space is implemented.

The water column is divided into a large number of layers with equal thicknesses; this thickness is also used as the depth increment in the calculations. Generally, the resolution of the modeling improves with a finer depth increment. Typically, the layer thickness is chosen to be about 1%, or less, of the water depth.

In each of these thin layers, the sound speed is approximated to a straight line, whereby the sound paths become segments of circular arcs. Going from layer to layer, the complete trajectory of the rays is easily determined, together with the travel times and information on where the rays have been reflected from the surface and bottom or gone through turning points. This information, the ray history, is stored in the computer and used in all the following calculations of TL and time responses.

The initial ray tracing is done by launching a number of rays (typically 100 rays), with angles selected to cover the entire space between the source location and out to receivers on a horizontal line at the specified receiver depth. Note that the number of initial rays may be larger than the number shown in Fig. 2.

Based on the history of the initial rays, the program determines the trajectories, travel times, and amplitudes of all eigenrays, within the span of initial ray angles, connecting a source position to the receiver positions. The contributions of all the eigenrays are thereafter coherently summed to produce the frequency-domain transfer function for propagation between the source and receivers. The time response is subsequently calculated by multiplying with the frequency function of the source

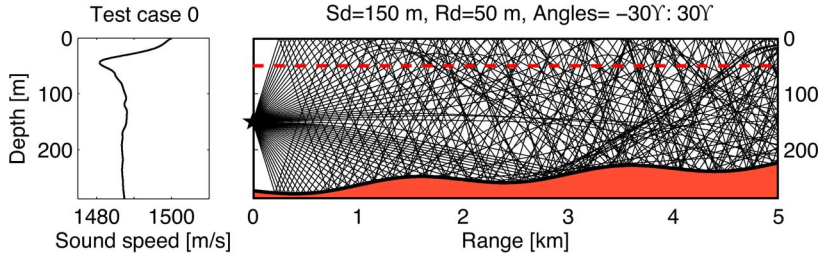

Fig. 2. Sound-speed profile and ray traces for a typical case. The source depth is 150 m and the receivers are all located on a horizontal line at 50-m depth, indicated by the dotted line. The initial angles of the rays at the source are from -30° to 30°.

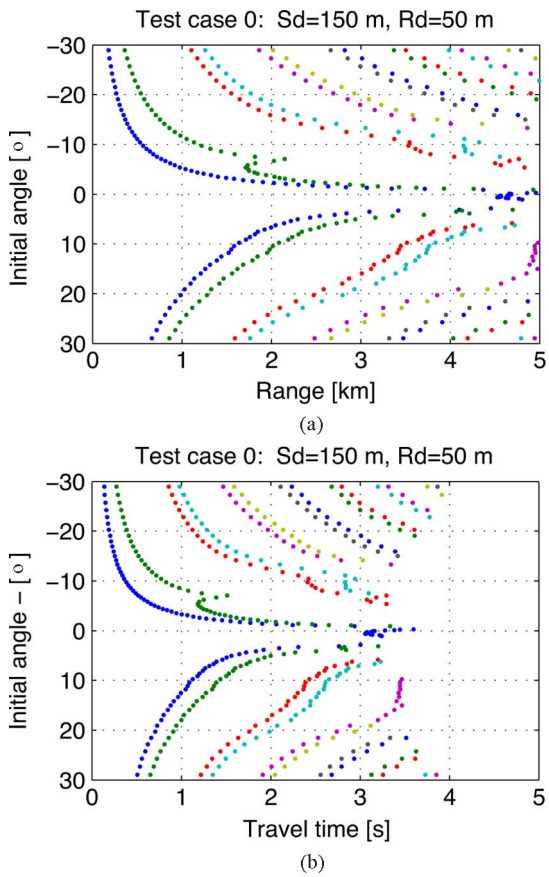

Fig. 3. Ray history of the initial ray tracing. (a) Range and (b) travel time as functions of initial ray angle at the source.

signal and Fourier transformation. Features of sound propagation that are important and relevant for the propagation of airgun signals to long distances in the water column are discussed in the following.

A. Eigenray Determination

The crucial task in ray trace modeling is to find all the eigenrays connecting a source position with the receiver positions. PlaneRay uses a unique sorting and interpolation routine that operates on the stored ray history resulting from the initial ray tracing; see Fig. 2 for an example.

Fig. 3 displays parts of the ray history showing the range and travel times to where the rays cross the receiver depth line (Fig. 2) as a function of the initial angle at the source. A particular ray may intersect the receiver depth line, at several ranges. For instance, the range-angle plot of Fig. 3 shows that at 2 km there are 11 eigenrays. The initial angles of these rays are approximately found from reading the plot to be 6°, 11°, 23°, and 25° for the positive (down-going) rays and -2°, -4°, -7°, -16°, -18°, -27°, and -29°, for the negative (up-going waves). However, the values found in this way are often not sufficiently accurate for the determination of the sound field. Therefore, further processing is needed to obtain more accurate results. The approach achieving the higher accuracy used in PlaneRay is based on sorting the different rays into groups or classes of similar ray history, followed by interpolation.

Fig. 4 shows an example of eigenray calculations with the eigenrays from a source at 50-m depth to a receiver at 150-m depth and distance of 3.5 km from the source.

B. Transmission Loss Calculation

In general, the sound attenuation in the ocean can be divided into three effects:

1) geometrical losses;
2) sound absorption in the water;
3) boundary losses from interactions with the sea surface and bottom.

1) Geometrical Losses: The acoustic intensity is calculated using the principle that the power within a space limited by a pair of rays with initial angular separation of $d\theta_0$ and centered on the initial angle θ_0 will remain between the two rays regardless of the rays' paths. The acoustic intensity $I(r)$ as a function of the horizontal range is, according to this principle, given by

$$I(r) = I_0 \frac{r_0^2}{r} \frac{\cos\theta_0}{\sin\theta} \left| \frac{d\theta_0}{dr} \right| \tag{3}$$

and the geometrical TL in respect to a reference distance r_0 of 1 m is

$$\mathrm{TL} = -20 \log_{10} \left[\frac{1}{r} \frac{\cos\theta_0}{\sin\theta} \left| \frac{d\theta_0}{dr} \right| \right]. \tag{4}$$

These equations predict infinite sound intensity under two conditions, when $\theta = 0$ and when $dr/d\theta_0 = 0$. The first condition signifies a turning point where the ray path becomes horizontal; the second condition occurs at points where an infinitesimal increase in the initial angle of the ray produces no change in the horizontal range traversed by the ray. The locations where $dr/d\theta_0 = 0$ are called caustics where infinite intensity is predicted. In reality, there is focusing of energy to a very high level, but the actual level is not determined by classical ray theory. The problem with calculating the acoustic field at caustics and turning points represents a limitation with ray theory.

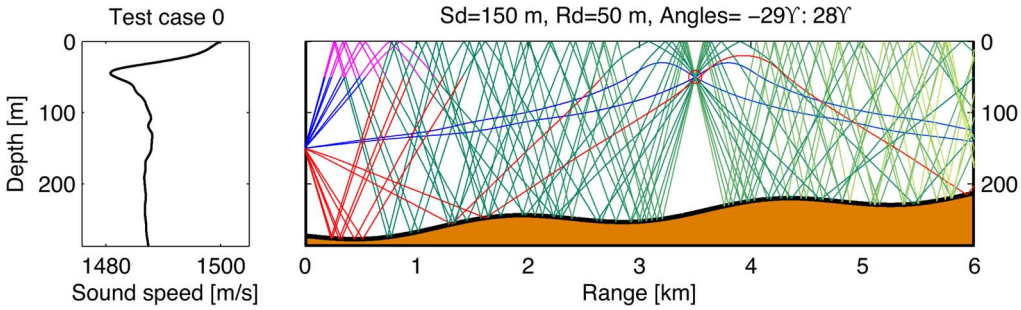

Fig. 4. Eigenrays from a source at 150-m depth to a receiver at 50-m depth and 3.5 km from the source.

Caustics may be caused by changes in the sound speed in the water column, or by changes in the bathymetry.

In free space, the geometrical loss is that of spherical spreading with which the sound intensity decays proportionally to distance squared. In a flat ideal waveguide, the geometrical loss follows a cylindrical spreading law since the sound pressure decays proportionally with distance. It follows that the geometrical spreading in a waveguide such as the sea, with constant sound speed, follows a spherical spreading law at short distance and cylindrical spreading at longer distance. A combination of the two spreading laws may be used for both short and long distances and expressed by

$$\mathrm{TL} = 10\log_{10}\left[r^2\left(1+\frac{r^2}{r_t^2}\right)^{-\frac{1}{2}}\right]. \tag{5}$$

This expression gives the asymptotic behavior

$$\mathrm{TL} = \begin{cases} 20\log_{10}(r), & r \le r_t \\ 20\log_{10}(r_t) + 10\log_{10}\left(\frac{r}{r_t}\right), & r > r_t. \end{cases} \tag{6}$$

In these equations, r_t is a transition range where the TL goes from spherical close to the source and to cylindrical at long ranges. A reasonable value for r_t is a value close to the water depth.

The cylindrical spreading law applies to an ideal waveguide with perfectly reflecting boundaries. Such conditions are often encountered in the oceans for sound that strikes the bottom at angles smaller (closer to horizontal direction) than the critical angle. The critical angle is given by the ratio of the sound speed c_w in the water to the sound speed c_b in the bottom by

$$\cos(\theta_{\mathrm{crit}}) = \frac{c_w}{c_b}. \tag{7}$$

Typically, the sound speed in a sedimentary bottom may be about $c_b = 1700$ m/s, which with a water sound speed of 1500 m/s gives a critical angle of about 28°.

Another geometrical asymptotic TL relation may result from destructive interference between the direct and surface-reflected signal resulting in

$$\mathrm{TL} = -40\log_{10}(r). \tag{8}$$

This interference is called the *Lloyd mirror effect* and is significant when the water is much deeper than the source and receiver depths. The bathymetry may also have considerable effects on the TL. This is demonstrated and discussed in connection with the analysis of the field trials.

2) Sound Absorption in Water: Viscosity is the main contribution to absorption in fresh water resulting in an absorption that increases proportionally with frequency squared. In seawater, there are also other relaxation phenomena that make important contributions to absorption losses. From [8] and [9], we find that the attenuation is around 0.001 and 0.1 dB/km at 100 and 1000 Hz, respectively. These values indicate that for the frequencies and ranges of interest in this discussion the absorption is not important, but it is included in the model.

3) Boundary Losses: Boundary losses are the reflection losses when sound strikes the sea surface or bottom. A flat sea surface totally reflects the sound waves, but at a rough sea surface there is a reflection loss that depends on the waves, the acoustic frequency, and the angle of incidence. The bottom reflection loss depends on the geological compositions and structure of the bottom, and the roughness.

Fig. 5 shows an example of the bottom reflection loss as a function of angle and frequency for a bottom with a sediment layer with the thickness $D = 10$ m. We assume the sediment layer consists of gravel, while the solid half-space is granite. From [10] and [11], we find the following parameters for the sediment layer: density 1700 kg/m^3 and sound speed 1700 m/s. The homogeneous solid half-space is found to have a sound speed of 2500 m/s, shear speed of 750 m/s, and a density of 2500 kg/m^3. All wave attenuations are 0.5 dB/λ as described by Hamilton [10], where $\lambda = c/f$ is the wavelength of the sound. For frequencies below 50 Hz, the critical angle is 55° and given by the compressional wave speed of the solid half-space. At higher frequencies, the critical angle is given by the sediment layer and is 28°. For angles lower than the critical angle, the reflection loss is ideally zero, i.e., total reflection, but absorption and conversion to shear wave energy results in reflection loss that may be significant, especially for signals undergoing multiple reflections at the bottom.

C. Time and Frequency Responses

This study uses a 50-Hz Ricker pulse as the input to the model as representative for the transmitted airgun pulse. The Ricker pulse is often used when modeling seismology [12]. Fig. 6 shows the pulse and its frequency spectrum. In the subsequent modeling, the peak amplitude is scaled up to the actual value used in the survey.

Fig. 7 shows the TL as a function of the range for the frequencies listed in the legend, and Fig. 8 shows the time response as a function of the distance with the transmitted source signal of Fig. 6. Both figures are for the scenario depicted in Fig. 2 with

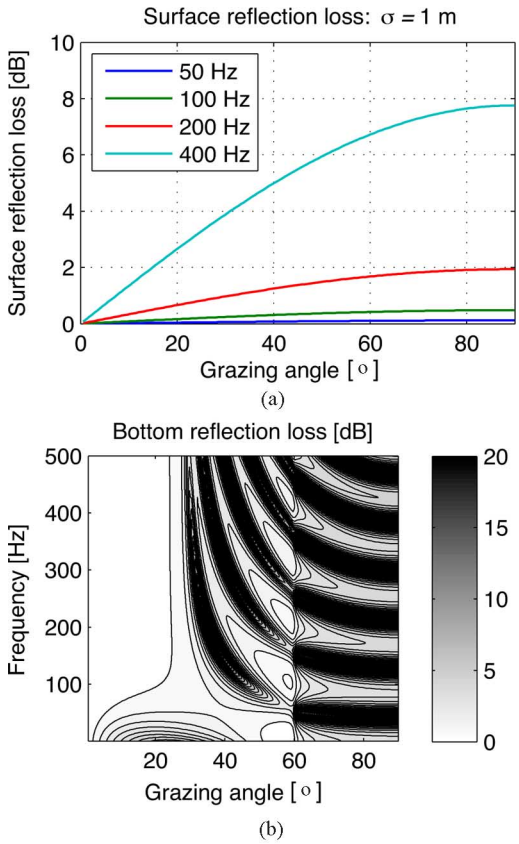

Fig. 5. Example of boundary reflection losses. (a) The surface reflection loss function of grazing angle, calculated for a wave height of 1 m and the frequencies of 50, 10, 200, and 400 Hz. (b) Bottom reflection loss for a bottom with a soft sediment layer over a solid half-space.

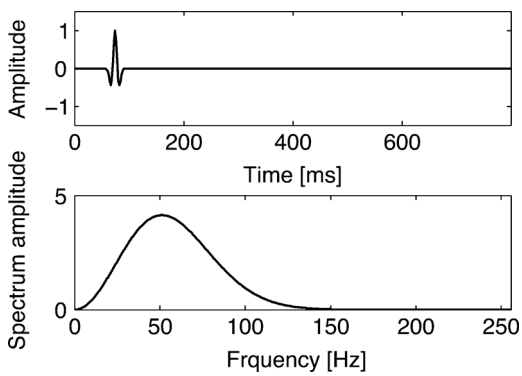

Fig. 6. A Ricker pulse and its frequency spectrum used in the model study.

the bottom being as described above. The time axis is reduced time, which is defined as

$$t_{\text{red}} = t_{\text{real}} - \frac{r}{c_{\text{red}}} \tag{9}$$

where t_{real} is the real time, r is the range, and c_{red} is the reduction speed. The actual value of c_{red} is not important as long as the chosen value results in a good display of the time responses. In our modeling, the reduction speed is 1500 m/s.

A unique feature of the PlaneRay code is that the various multipath contributions are calculated independently and these are shown in Fig. 8(a). Addition of all the multipath contributions

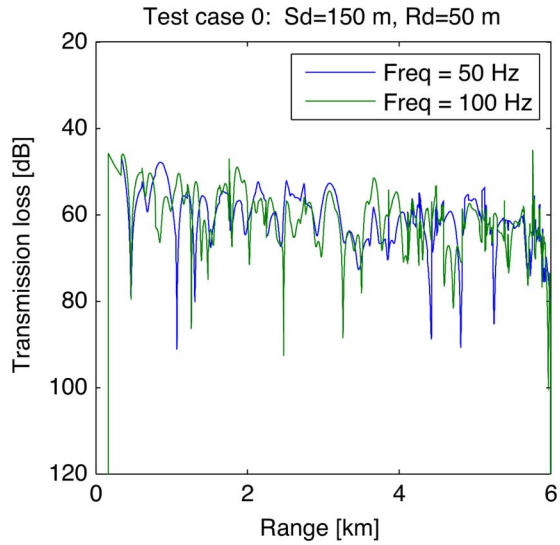

Fig. 7. Transmission loss in decibels as a function of the range for the scenario of Fig. 2 and with a homogenous fluid bottom with sound speed of 1700 m/s, density of 1700 kg/m^3, and attenuation of 0.5 dB/λ.

results in the total time response shown in Fig. 8(b). Note that the time responses [Fig. 8(a)] show particular high sound levels at approximately 2 and 5 km. These peaks in sound level are caused by caustic; the first is a caustic by the sound speed and the other is a caustic by changes in the bathymetry.

D. Modeling Array Directivity

A typical layout used in commercial seismic surveys is shown in Fig. 9 with N_x guns in the towing direction and N_y guns in the cross direction. Typically, there may be around 30 active guns of different sizes distributed over an area of 20 m × 25 m. Considering the size of the airgun array and the wavelengths, it is clear that the directivity of the airgun array must be included in the calculations of the acoustic field. The program is constructed in such a way that any source directivity can be introduced in the calculation by modifying a subroutine that produces the beam pattern $B(\omega, \theta)$ as a function of (angular) frequency ω, applied to the field contribution of each eigenray with initial elevation angle θ.

With reference to Fig. 9, the positions of the guns are denoted by (x_n, y_m) and source strengths are $Q_{n,m}(\omega)$. The signal from the array in the far field as a function of the elevation angle θ, the azimuth angel φ, and the (angular) frequency ω can be expressed as

$$S(\omega, \theta, \varphi) = \sum_{n,m} Q_{n,m}(\omega) e^{-\frac{\omega}{c} i(x_n \cos\theta \cos\varphi + y_m \cos\theta \sin\varphi)}. \tag{10}$$

In the in-line direction where the azimuth angel φ is zero, this reduces to a line array of sources

$$S(\omega, \theta, \varphi = 0) = \sum_{n,m} Q_{n,m} e^{-\frac{\omega}{c} i(x_n \cos\theta)}. \tag{11}$$

Equations (10) and (11) are general expressions valid for any number of sources with different frequency spectrum and locations, but require that the source functions be known for each of the guns in the arrays. In cases that such detailed information

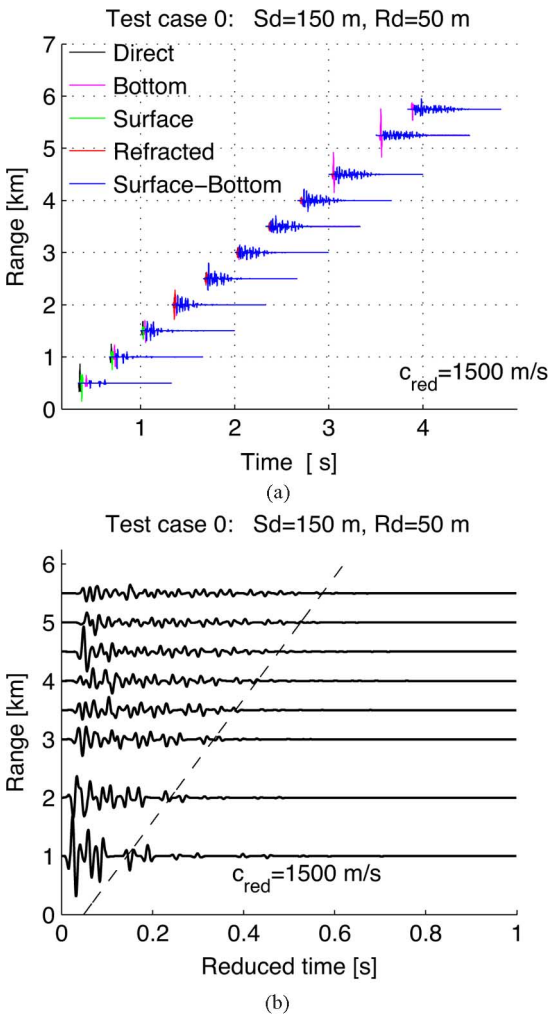

Fig. 8. Time responses as a function of the range plotted as a function of the reduced time. (a) Plot of the individual multipath contributions. Direct: Direct sound. Bottom: One bottom reflection. Surface: One surface reflection. Refracted: One turning point due to sound speed. Surface Bottom: Several surface and bottom reflections. The signals have been compensated for cylindrical spreading. In PlaneRay, there is also a last group of signals called "Other," where all other multipaths are grouped. Since no rays were in this group it was excluded from the plot. (b) Plot of the total time responses as a function of the reduced time. The total time response is made of a coherent summation of all individual multipath contributions.

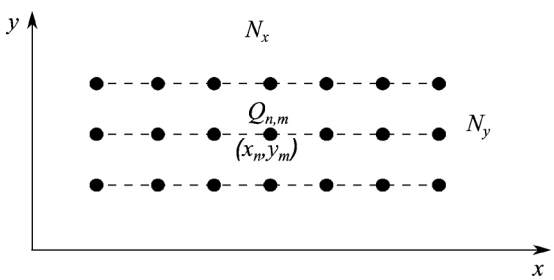

Fig. 9. Airgun array with N_y lines each with N_x guns.

is not available, the following approach is used to estimate the directivity function of the airgun array. The approach is based on the assumption that all the guns in the array produce pulses

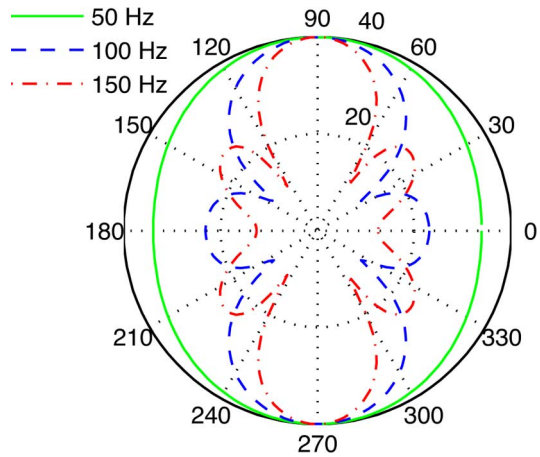

Fig. 10. Modeled directivity of the airgun array for 50 and 100 Hz. The calculated directivity pattern is for the weights and positions of the airguns used by the vessel *Geo Pacific* in the seismic survey in Vesterålen during summer 2009.

of the same shape, but with a peak pressure amplitude that depends only on volume of the pressure chamber, given that the pressures in the guns are all the same.

Thereby, the source strengths in the above equations for the beam pattern are replaced by volume weights

$$Q_{n,m}(\omega) = Q_0(\omega) V_{n,m}^{\gamma}. \tag{12}$$

In this expression, $V_{n,m}$ is the normalized volume of the individual guns and the exponent γ has the value of 1/3 [13]. $Q_0(\omega)$ is a frequency function of the common source signal, which here is taken as a Ricker pulse as previously described.

The in-line direction of the transmitted signal from the array is then given as

$$S(\omega, \theta, \varphi = 0) = Q_0(\omega) \sum_{n=1}^{N_x} q_n e^{-\frac{\omega}{c} i (x_n \cos\theta)} \tag{13}$$

where q_n represent the relative strengths of the individual guns and x_n are their positions along the x-axis. The far-field beam pattern as a function of elevation angle and frequency is given by

$$B(\omega, \theta) = \sum_{n=1}^{N_x} q_n e^{-\frac{\omega}{c} i (x_n \cos\theta)}. \tag{14}$$

In the current situation, this resulted in a line array (x_n in meters)

$$\begin{aligned} q_n &= [0.2308 \quad 0.1963 \quad 0.1679 \quad 0.1656 \quad 0.1350 \quad 0.1044] \\ x_n &= [0 \quad 5.0 \quad 7.5 \quad 11.0 \quad 13.0 \quad 16.0]. \end{aligned} \tag{15}$$

Fig. 10 shows the resulting beam pattern for the frequencies of 50 and 100 Hz. For 50 Hz, the reduction in the transmitted level in the horizontal directions is about 5 dB compared to the level in the vertical direction. At higher frequencies, there is a sidelobe structure that for 100 Hz has a level of about -15 dB compared with the level in vertical direction. The maximum amplitude is in the vertical direction and in the modeling of the

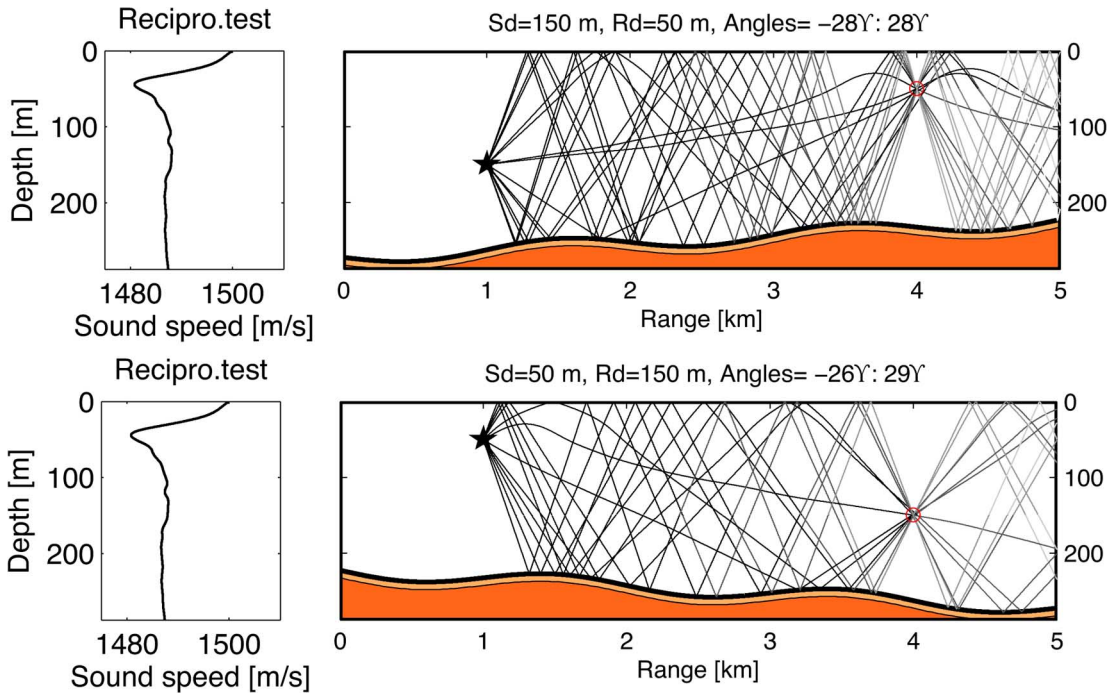

Fig. 11. Transmission over an undulating sloping bottom with a northern summer sound-speed profile with the eigenrays for the two reciprocal situations.

time and frequency responses the maximum peak amplitude is scaled up to the level specified by the surveyor, which is 255 level re 1 μPa in the case reported here.

E. The Reciprocity Principle

The principle of reciprocity is an important and useful property of linear acoustics and systems theory. The principle of reciprocity stipulates that the sound pressure at a position B due to a source at position A is equal to the pressure at A due to a similar source at B. The principle is very general and valid also in cases where the wave undergoes reflections and refraction at boundaries on its path from the source to the receiver [14]. To demonstrate the reciprocity principle in practice, we chose the same scenario as before (Fig. 2). In the actual situation, the source is located at 150-m depth and the receiver at 50 m. In the reciprocal situation, the source and receiver depths are interchanged and the bathymetry is flipped. The eigenrays for the two reciprocal situations are shown in Fig. 11 where the two ray diagrams show the most significant eigenrays. In this example, the bottom is modeled with a 10-m-thick sediment layer over a homogenous solid half-space. The sedimentary layer has a sound speed of 1700 m/s, attenuation 1 dB/λ, and density of 1500 kg/m^3. The solid half-space has a compressional sound speed of 2500 m/s, a shear speed of 750 m/s, and the density is 2500 kg/m^3. All waves have absorptions of 0.5 dB/λ.

Fig. 12 presents the modeled time response for the two situations where the source emits a short Ricker pulse with main frequency 50 Hz. The two signals are very similar, and the error, defined as the difference in energy between the two signals, is less than 10%. The reciprocity principle may be used for checking the validity of the model. It is a good indication that the model result is correct if modeling the real case and the reciprocal situation yield the same results.

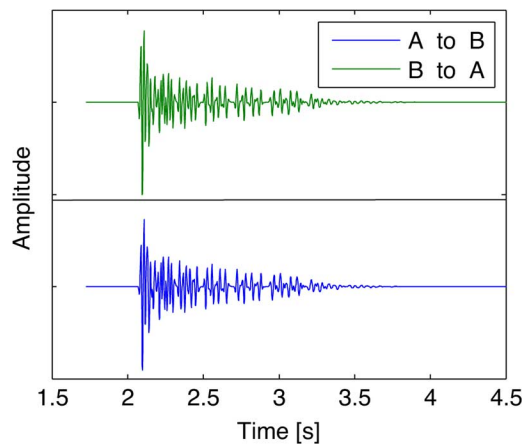

Fig. 12. Time signal from a source at position A (150 m) to the receiver at position B (50 m) compared with the reciprocal situation with transmission from B to A.

F. Characterization of Transient Noise

The airgun signals are transient pulses, which require different characterization and measures than continuous noise. Following [15], the following matrices can be used to characterize the impulse signals from airguns.

The sound exposure level (SEL) is an energy-based measure of noise used to compare noise events of different length. The SEL value is equal to the level of a continuous noise of 1-s duration, defined as

$$\mathrm{SEL} = 10\log_{10}\left(\frac{E_x}{E_{\mathrm{ref}}}\right) = 10\log_{10}\left(\frac{E_x}{p_{\mathrm{ref}}^2 t_{\mathrm{ref}}}\right). \quad (16)$$

The energy E_x (omitting the impedance that disappears in the subsequent normalization) is defined as

$$E_x = \int_0^T p^2(t)dt. \quad (17)$$

The reference pressure $p_{\rm ref}$ is equal to 1 μPa and $t_{\rm ref}$ is 1 s. SEL has the unit dB re (1 μPa^2)(1 s).

Peak pressure level (PPL) is a descriptor used to compare the maximum peak level of noise exposures. The PPL is defined as

$$\mathrm{PPL} = 20\log_{10}\left(\frac{|p_{\max}|}{p_{\rm ref}}\right) \tag{18}$$

where $|p_{\max}|$ is the maximum peak value (absolute), and $p_{\rm ref}$ is equal to 1 μPa. One should be aware that the maximum peak pressure is not a sound field characteristic, but a time–space varying consequence of the coherent effects of multipath effects and bandwidth.

These measures are applied to the time traces of Fig. 8 and the results are displayed in Fig. 13. There are several features that stand out. First, the general trend at long ranges is that the SEL tends to fall with approximately $10\ \log(\mathrm{r})$ and that PPL falls with $20\ \log(\mathrm{r})$ or with cylindrical and spherical spreading for the energy and for the peak level, respectively. This is a general feature that applies to most waveguide propagation situations where the bathymetry is reasonably constant and where sound absorption in the water plays a minor role. Consequently, the ratio between the peak sound pressure and, for instance, the root mean square (RMS) pressure is not constant, but will generally vary with distance. Second, there are a number of peaks that reach significant higher values. These are caused by the sound-speed profile and the refraction effects at caustics and turning points.

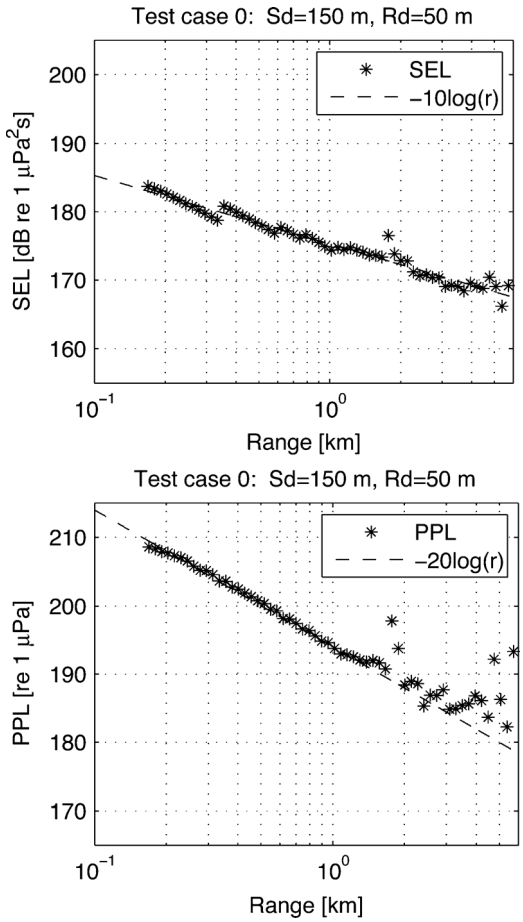

Fig. 13. Sound exposure level and peak pressure level as a function of the range calculated for the scenario shown in Fig. 2.

IV. The Nordland VII Field Experiment

The Norwegian Petroleum Directorate (NPD) conducted a seismic survey about 15 km off the coast of Vesterålen (northern Norway) in summer 2009 (Fig. 14). The survey area was 15 km $\times$ 85 km and overlapped parts of both the continental shelf and the slope. Seismic data were collected along a total of 41 lines (transects) with a distance of 400 m between adjacent transects. The airgun shooting was carried out according to standard procedure for 3-D-seismic surveys using two airgun arrays (57.4 L each) that were discharged about every 10 s (flip-flop).

In connection with this seismic survey, a project was carried out by the Institute of Marine Research (IMR, Bergen, Norway) to study how airgun discharges during the survey affected fish distribution and the commercial fisheries in the area [16]. Fishing vessels (gillnet and longline boats) were chartered to fish for Greenland halibut, redfish, saithe, and haddock before, during, and after the seismic data acquisition. A research vessel carried out an acoustic survey of the distribution of fish in the area to determine whether this changed when the seismic airgun discharges started.

During the seismic survey, IMR also collected calibrated sound recordings of airgun sounds. The recordings were made by several standalone self-recording hydrophone platforms located on the seabed at a range of depths and distances from the seismic transects. Each hydrophone platform was equipped with a Naxys 02345 Ethernet hydrophone connected to an underwater housing that contained batteries and a computer for data logging (for details, see [17]). The platform was made buoyant with floats and was attached to weights (100 kg) with a 3-m rope. An acoustic release unit attached to the rope enabled retrieval of the unit when sound recordings were accomplished.

The line chosen for the analysis and comparison with the model is the section of the line indicated by the solid part of the red line in Fig. 14. This line, referred to as line 1344, is about 30 km long and passing directly above one of the hydrophone positions. These data have been used for comparison with the modeled results using the acoustic propagation model described earlier. The data used for the comparison were recorded on a single hydrophone at a depth of 83 m receiving signals from a moving and approaching source at 6-m depth. As a practical matter, it is easier to model the reciprocal situation with flipped bathymetry and with a source at 83 m and a line of receivers at 6-m depth. The modeled "flip scenario" is shown in Fig. 15.

A. Measured and Modeled Sound Levels

The sound-speed profile is a typical profile measured in the area at the time of the survey. The water depth varied significantly along the line, from 100-m to more than 200-m depth and with maximum slopes of approximately 2%. Based on available information of the geology, the bottom was modeled as a homogenous solid with compressional wave speed 2000 m/s, shear wave speed 600 m/s, and density 2500 kg/m^3. The compressional wave attenuation was set to 0.1 dB/λ, and the shear wave attenuation was set to 1 dB/λ. No attempts were made to optimize the seabed parameters to obtain better agreement

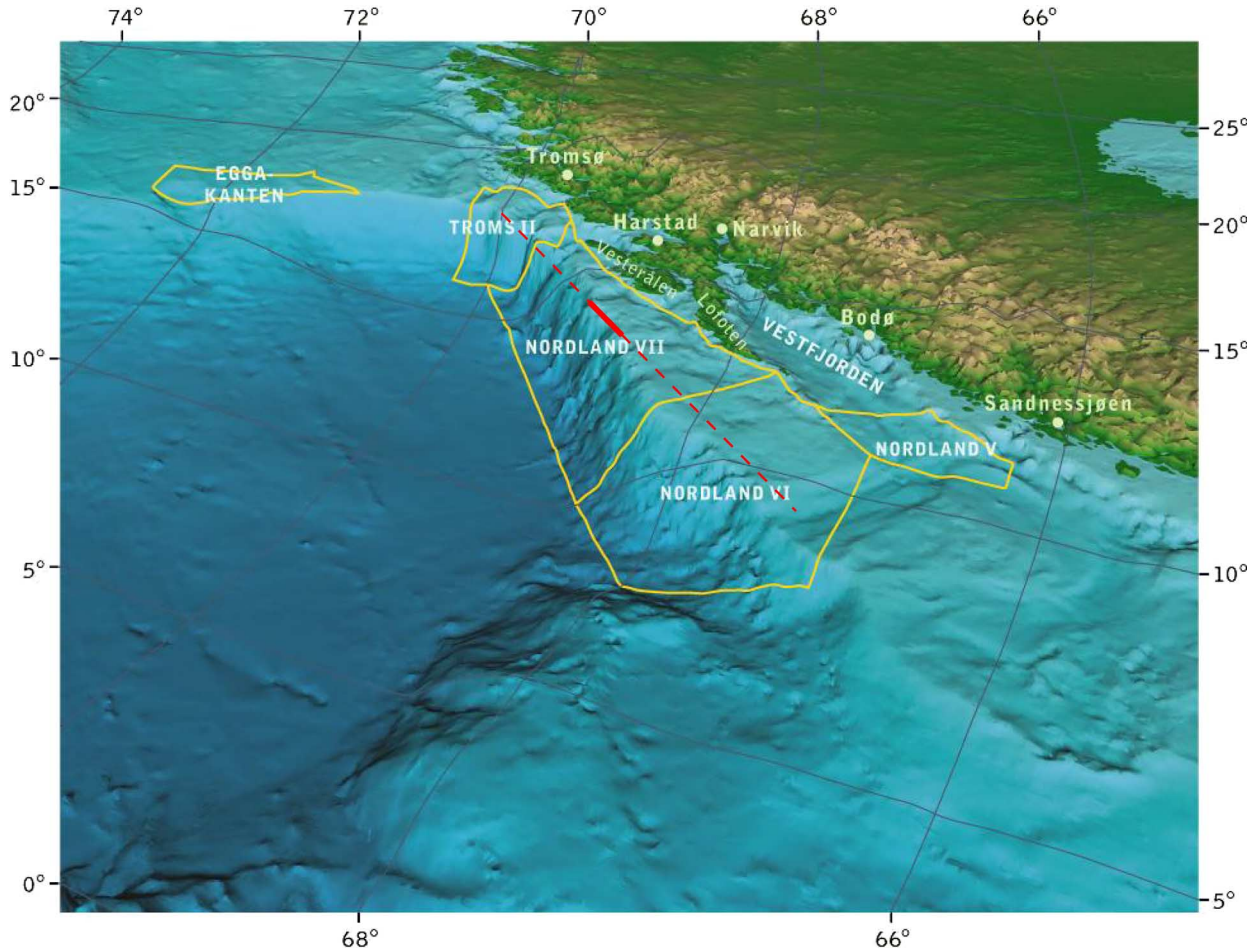

Fig. 14. The area of the seismic experiment in summer 2009. The acoustic data were recorded with the seismic vessel traveling the 30-km section indicated with the solid part of the black line. Picture from the Norwegian Petroleum Department (NPD) webpage.

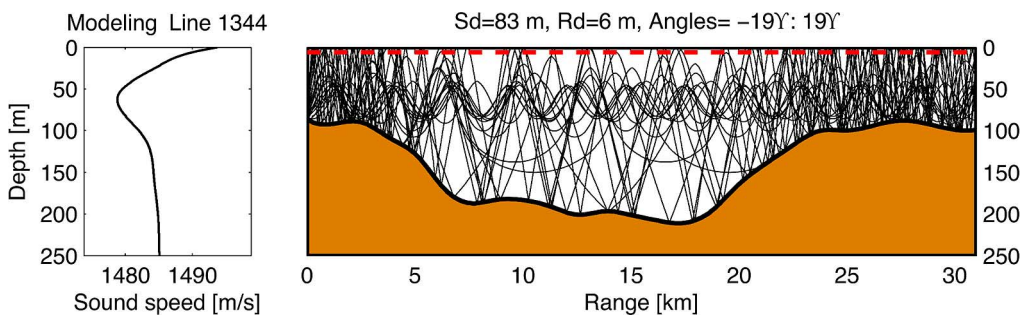

Fig. 15. The modeled "flip scenario" of line 1344 at Nordland VII. The sound-speed profile and the bathymetry. The receivers are at 6-m depth, the star is the source at 83 m, and the lines are the emanating rays from the source.

with measured values. Fig. 16 shows the TL as a function of the distance from the source. The impact of the changing water depth is very important. Until a distance of 2–3 km, the decay is about $-10\log(\mathrm{r})$; thereafter the water depth increases significantly and the decay approaches $-40\log(\mathrm{r})$. At the longest range, where the water becomes shallower, the sound level increases again.

The time responses are synthesized by multiplying the frequency function of the source function, which in this case was a Ricker pulse with peak pressure amplitude set to 255 level re 1 μPa, which is the value specified by the seismic company. Fig. 17 shows examples of measured and modeled time responses for distances up to 10 km. There are some common features in the overall structure such as time duration and the amplitude decay, but the details are different.

Fig. 18 shows the SEL and PPL values derived from the measured and modeled airgun sounds. Unfortunately, the recorded signals were saturated in the receiver at ranges less than about 1 km. This affects severely the peak levels, but not so much the SEL values. The general agreement between the measured and modeled results is good with both showing a significant decreasing level starting at a range of about 2 km. This behavior is attributed to the abrupt change in water depth at this range (see Fig. 15) and the modeled TL (see Fig. 16). The increased levels, due to the shallower water, from about 20 km are also present in both the measured and modeled results.

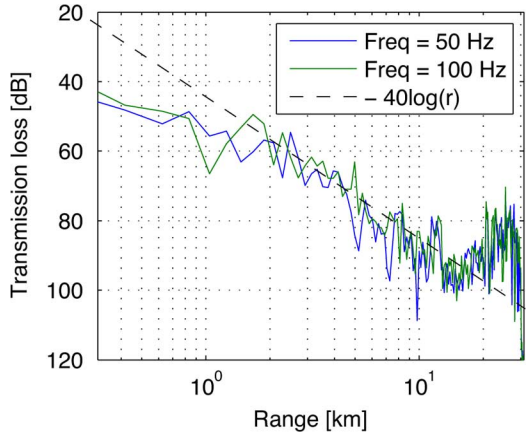

Fig. 16. Modeled transmission loss as a function of the distance from the source for the scenario shown in Fig. 15 and the frequencies given in the legend. The dotted line is $-40\log(\mathrm{r})$ introduced to facilitate the discussion in the text.

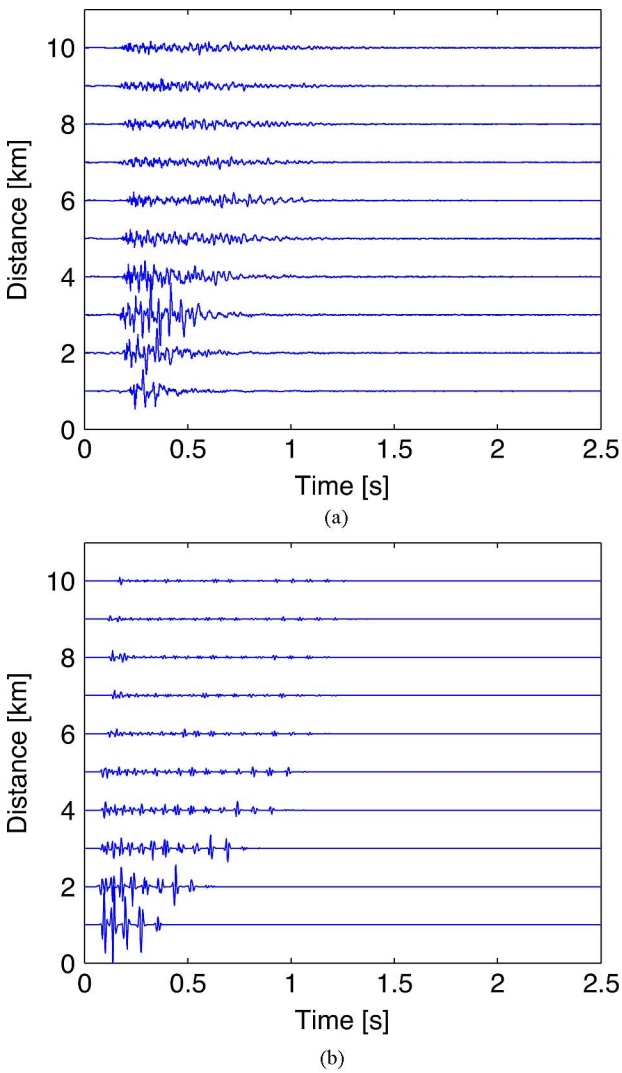

Fig. 17. (a) Measured and (b) modeled time responses as a function of the distance of up to 10 km. The measured signals are aligned by their maximum peak value and compensate for geometrical spreading.

In general, the modeled PPL values are higher than the measured values over the whole range of distances. Such a systematic difference may be explained by several factors. The simplest explanation is that the maximum peak level of 255 re 1 μPa, which was not measured, but taken from the specifications, is not correct. Another possibility is that the effect of directivity is overestimated and that the array in fact is more omnidirectional than the directivity of Fig. 10, which is used in the modeling. There is also evidence that the airgun signals are richer in low-frequency content, below 50 Hz, than the 50-Hz Ricker pulse used in the modeling resulting in a lower effective directionality than assumed. This last factor can also explain the underestimation that appears in the deep-water region. Another possible explanation is that the bottom sediment changes along the shooting line. When the water depth changes abruptly it is likely that the sediment type also changes. This can lead to both higher and lower absorption and/or reflection and is not taken into account in the model. Abrupt change in water depth will also, unquestionably, change the sound-speed profile. Since the model only includes the depth-dependent sound-speed profile, not distance-dependent one, this will also affect the results.

B. Startle Threshold and Critical Range

The ultimate goal of the project is to be able to estimate the minimum distance from a seismic survey to avoid significant negative effects on fish behavior and fish catch. This is a difficult task that requires knowledge about hearing sensitivity and behavior reactions in different species of fish. This is not the subject of this paper, but we demonstrate how knowledge of fish sensitivity and reaction to anthropogenic sound may be used in the acoustic model to calculate the minimum distance.

The Institute of Biology at the University of Oslo (Oslo, Norway) has recently studied startle response thresholds in different species and auditory groups of fish to short duration (30–500 ms), single-tone sound pulses of varying frequencies and pressure levels [18]. Small groups (2–4) of fish such as Atlantic cod (*Gadus morhua*) and others were examined in a specially designed pressure chamber, and startle threshold values were obtained using a 10% response criterion. Thus, at threshold stimulation, on average, one out of ten fish showed fright behavior in the form of a C-type startle response. For Atlantic cod (Fig. 19), startle threshold values were 60–70 dB above known auditory thresholds in codfish (family Gadidae). It should be noted that in addition to peak pressure levels, startle thresholds were found to depend on the rise time of the sound pulses. As a consequence, behavior pressure thresholds are expected to rise with increasing sound source distance. This factor may be important in the field, but for clarity, it has not been modeled in this study.

We define the *critical distance* in a given species of fish as the maximum distance where SPL exceeds startle response threshold. To calculate critical distances, the time responses from both measurements and modeling results were transferred to the frequency domain and compared to the determined startle response thresholds for Atlantic cod. Fig. 20 shows the results for the measured and modeled levels for line 1344 as contour plots with frequency and range as the y- and x-axis, respectively. The main plateau of sound levels exceeding the startle threshold values extends out to approximately 5 km (see the green lines in Fig. 20), which thus is the critical distance resulting from both measured and modeled sound fields. However, it should be noted that startle thresholds may

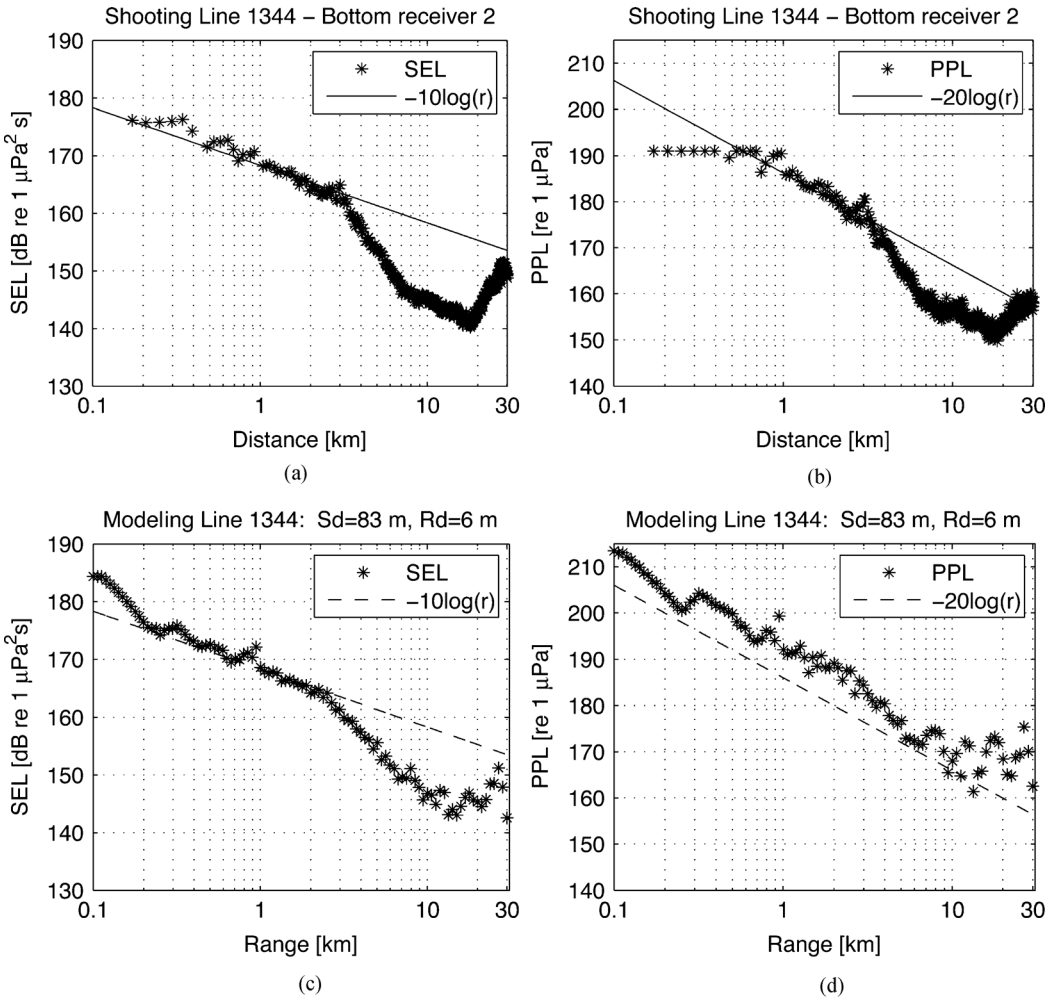

Fig. 18. SEL and PPL from the measured and modeled airgun sounds of line 1344 at bottom receiver at a depth of 83 m. The plots show the (a) measured SEL, (b) measured PPL, (c) modeled SEL, and (d) modeled PPL. In the measured signal, the signal is clipped at 191 dB, hence the distances below 1 km may not be correct. The dashed lines represent the decay rates of $10\log(\mathrm{r})$ and $20\log(\mathrm{r})$.

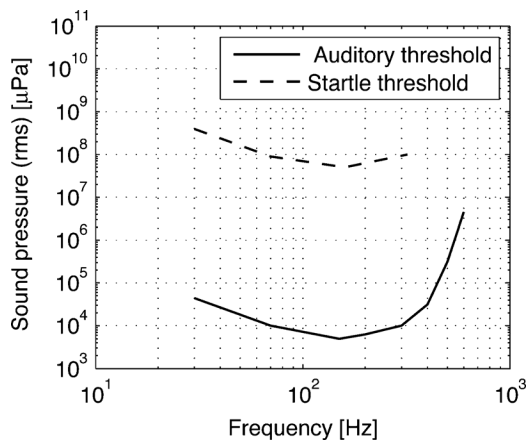

Fig. 19. Startle response pressure thresholds (mean values) recorded in Atlantic cod and average auditory thresholds in Gadidae [3], [19]. Atlantic cod sizes in the startle experiments were 15–22 cm.

vary depending on factors such as background noise levels and that they depend on additional components of seismic pulses besides p-p pressure levels.

The difference between the measured and modeled results is primarily in the frequencies outside the 50-Hz Ricker pulse bandwidth. This also affects the lines indicating where the threshold is exceeded. Another observation is the underestimation of SPL in the deep water (from approximately 5 to 20 km). This is most clear when observing the −3- and −6-dB threshold lines.

It is also possible to observe the increased sound levels above 20 km. This can be found in both measured and modeled results.

V. Discussion and Summary

This paper has described and demonstrated an acoustic ray tracing model for simulating the propagation of airgun sound in the water column. The modeled results are compared with measured acoustic sounds obtained at a joint seismic–acoustic survey at the field Nordland VII in Vesterålen, Norway, during summer 2009. Model results have been compared with recorded airgun sounds received on a hydrophone near the bottom at 83-m depth as a function of the distance of up to 30 km. The water depth changes quite significantly along the 30-km line and this has a strong impact on the propagation of airgun sounds.

Quantitatively, the modeled and measured sound levels are compared based on two measures: the SEL which is an energy measure, and the PPL. The agreement between the measured

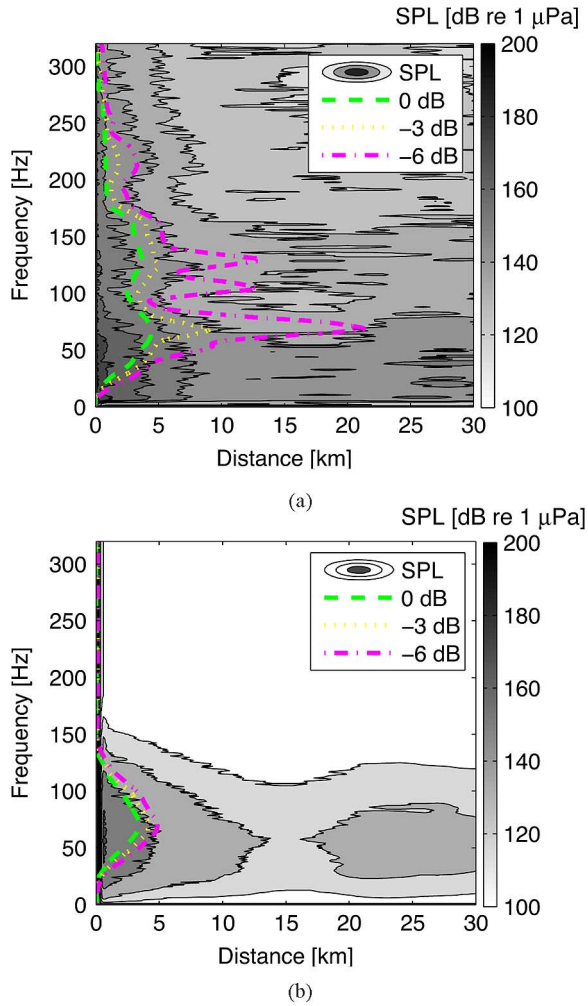

Fig. 20. Acoustic startle response thresholds in Atlantic cod compared to (a) measured and (b) modeled pressure levels for line 1344 at Nordland VII. The critical distance was approximately 5 km in both situations. The lines are the maximum distance where the startle thresholds are exceeded. Startle threshold according to the specified limits. The bottom parameters used in the modeling are: compressional wave speed: 2000 m/s; bottom density: 2 500 kg/m^3; compressional wave attenuation: 0.1 dB/λ; shear wave speed: 600 m/s; and shear wave attenuation 1 dB/λ.

and modeled levels is good with both revealing strong bathymetric effects.

The ultimate goal of the project is to be able to estimate the minimum distance from a seismic survey to avoid that fish react in a way that may affect the fishing. At a distance of about 5 km, the sound level was determined to be equivalent to the threshold value for startle response in cod. Acoustic startle responses are strong with rapid escape reactions directed away from the sound source [20], [21], but the fish are likely to show other types of behavioral changes at lower sound levels than those causing startle responses. Pearson *et al.* [22] studied behavioral changes in rockfish (*Sebastes spp.*) exposed to airgun sounds, and the threshold for alarm responses (increases in activity and changes in schooling and water position) was observed at 20–25 dB lower than the threshold for startle responses. Therefore, fish may respond and change behavior at lower sound levels, i.e., at longer distances, than those eliciting startle responses. On the other hand, increased rise time of sound pulses has been shown to increase acoustic startle response thresholds in fish [18], [23]. Distant and more drawn out sound pulses may thus be of less behavioral importance to fish than sharply rising pulses revealing a close-by sound source.

The values for "affect" distances quoted in this paper are only indicative and only intended to describe the approach and potential of the model. This study is the first to combine advanced acoustic propagation modeling with knowledge of fish hearing sensitivity and reaction to actually produce an estimate of the minimum distance between seismic shooting and fish populations to prevent changes in the behavior.

References

[1] J. R. Nedwell, K. Needham, A. W. H. Turnpenny, and D. Thomson, "Measurement of sound during a 3D seismic survey in blocks 14/14a of the North Sea," Subacoustech Limited, Hants, U.K., Subacoustech. Rep. Reference 356R0108, 1999.

[2] F. B. Jensen, W. A. Kuperman, M. B. Porter, and H. Schmidt, *Computational Ocean Acoustics*. New York: AIP Press, 1993, ch. 3–7.

[3] C. J. Chapman and A. D. Hawkins, "A field study of hearing in the cod, Gadus morhua," *J. Comparative Physiol.*, vol. 85, pp. 147–167, 1973.

[4] A. N. Popper, R. R. Fay, C. Platt, and O. Sand, "Sound detection mechanisms and capabilities of teleost fishes," in *Sensory Processing in Aquatic Environments*, S. P. Collin and N. J. Marshall, Eds. New York: Springer-Verlag, 2003, pp. 1–38.

[5] J. M. Hovem, "PlaneRay: An acoustic underwater propagation model based on ray tracing and plane wave reflection coefficients," in *Proc. Theor. Comput. Acoust.*, M. Taroudakis and P. Papadakis, Eds., Crete, Greece, 2008, pp. 273–289.

[6] *"OASES Version 3.1 User Guide and Reference Manual,"* H. Schmidt, Ed., Dept. Ocean Eng., Massachusetts Inst. Technol. (MIT), Cambridge, MA, 2004.

[7] J. M. Hovem, "PlaneRay, An acoustic underwater propagation model based on ray tracing and plane-wave reflection coefficients," Forsvarets forskningsinstitutt/Norwegian Defence Research Establishment, Horten, Norway, FFI Rep. 08/00610, 2010.

[8] R. E. Francois and G. R. Garrison, "Sound absorption based on ocean measurements. Part I: Pure water and magnesium sulphate contributions," *J. Acoust. Soc. Amer.*, vol. 72, no. 3, pp. 896–907, 1982.

[9] R. E. Francois and G. R. Garrison, "Sound absorption based on ocean measurements. Part II: Boric acid contribution and equation for total absorption," *J. Acoust. Soc. Amer.*, vol. 72, pp. 1879–1890, 1982.

[10] E. L. Hamilton, "Acoustic properties of sediments," in *Acoustics and Ocean Bottom*, L. Lara-Sáenz, C. Ranz-Guerra, and C. Carbó-Fité, Eds. Madrid, Spain: Consejo Superior de Invertigaciones Cientificas (CSIC), 1987, pp. 3–58.

[11] E. L. Hamilton and R. T. Bachman, "Sound velocity and related properties of marine sediments," *J. Acoust. Soc. Amer.*, vol. 72, no. 6, pp. 1891–1904, 1982.

[12] R. E. Sheriff and L. P. Gelhart, *Exploration Seismology*, 2nd ed. New York: Cambridge Univ. Press, 1994, p. 183.

[13] J. Caldwell and W. Dragoset, "A brief overview of seismic air-gun arrays," *The Leading Edge*, vol. 19, no. 8, pp. 898–902, 2000.

[14] L. D. Landau and E. M. Lifshitz, *Fluid Mechanics*. New York: Pergamon, 1959, p. 290.

[15] W. M. Carey, "Sound sources and levels in the ocean," *IEEE J. Ocean. Eng.*, vol. 31, no. 1, pp. 61–75, Jan. 2006.

[16] S. Løkkeborg, E. Ona, A. Vold, and A. Salthaug, "Sounds from seismic air guns: Gear- and species-specific effects on catch rates and fish distribution," *Can. J. Fish. Aquat. Sci.*, vol. 69, no. 8, pp. 1278–1291, 2012.

[17] J. T. Øvredal and B. Totland, "Sound recording systems for measuring sound levels during seismic surveys," in *Effects of Noise on Aquatic Life*, A. N. Popper and A. Hawkins, Eds. New York: Springer Science/Business Media, 2011, pp. 481–484.

[18] H. E. Karlsen and J. R. Eckroth, "Terskelverdier for Lydpulsindusert Startle-Atferd Hos Ulike Arter og Hørselgrupper av Fisk, og Effekter av Lydpulser på Spisemotivasjon," Report to the Norwegian Petroleum Directorate, 2011.

[19] C. J. Chapman, "Field studies of hearing in teleost fish," *Helgoland Mar. Res.*, vol. 24, pp. 371–390, 1973.

[20] R. C. Eaton, J. G. Canfield, and A. L. Guzik, "Left-right discrimination of sound onset by the Mauthner system," *Brain Behav. Evol.*, vol. 46, pp. 165–179, 1995.

[21] H. E. Karlsen, R. W. Piddington, P. S. Enger, and O. Sand, "Infrasound initiates directional fast-start escape responses in juvenile roach Rutilus rutilus," *J. Exp. Biol.*, pp. 4185–4193, 2007, 2004.
[22] W. H. Pearson, J. R. Skalski, and C. I. Malme, "Effects of sounds from a geophysical survey device on behaviour of captive rockfish (Sebastes spp.)," *Can. J. Fish. Aquat. Sci.*, vol. 49, pp. 1343–1356, 1992.
[23] J. H. S. Blaxter, J. A. B. Gray, and E. J. Denton, "Sound and startle responses in herring shoals," *J. Mar. Biol. Assoc.*, vol. 61, pp. 851–869, 2011.

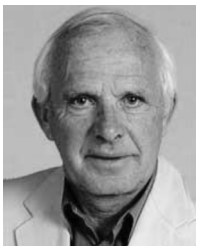

Jens M. Hovem (M'99) received the Ph.D. degree in communication theory from the Norwegian University of Science and Technology (NTNU), Trondheim, Norway, in 1966.

His experience includes two periods at SACLANT Undersea Research Centre (now NATO Undersea Research Centre, NURC, La Spezia, Italy), as a Scientist and Division Chief. In 1991, he was appointed Professor at the Department of Electronics and Telecommunication at NTNU conducting research and giving coursers in underwater acoustics and signal processing. He has been a Visiting Scientist at the Applied Research Laboratories (ARL), The University of Texas at Austin, Austin, in 1979 and 2002 and to CNRS Laboratoire de Mecanique et d'Acoustique, Marseilles, France, in 1998. He is now Professor Emeritus at the Department of Electronics and Telecommunication, NTNU, and senior advisor to SINTEF Information and Communication Technology (ICT), Trondheim, Norway. He is the author of the new book *Marine Acoustics—The Physics of Sound in Marine Environments* (Los Altos, CA: Peninsula Publishing, accepted for publication). His main fields of interest are underwater acoustics and signal processing.

Tron Vedul Tronstad received the M.S. degree in electronics engineering from the Norwegian University of Science and Technology (NTNU), Trondheim, Norway, in 2007. His specialization was acoustics and his M.S. thesis was on modeling of hearing damage in humans.

Currently, he is a Research Scientist at SINTEF Information and Communication Technology (ICT) Acoustics, Trondheim, Norway, where he works on acoustical topics both under water and in air. In the under water topic, his main field of interest is sound propagation in the water column.

Hans Erik Karlsen is an Associate Professor in Physiology at the University of Oslo, Oslo, Norway. He is currently the Director of Marine Biological Station Drøbak. His main field of interest is sound detection in fish and marine invertebrates.

Svein Løkkeborg received the Ph.D. degree in fisheries biology from the University of Bergen, Bergen, Norway, in 1990.

He has conducted many behavioral field investigations using underwater camera and telemetry technology to study swimming pattern, activity rhythms and foraging strategies in fishes and crabs. He has been involved in numerous fishing-gear-related studies including most fishing gears, and he has studied problems such as methods for fish abundance estimation, harvest strategies, selectivity, and bycatch. He has been working on three aspects related to ecosystem effects of fishing activities: mitigation measures to reduce bycatch of seabirds in longline fisheries, impacts of trawling on benthic communities, and lost fishing gears (ghost fishing). He has also been working on issues related to interactions between fishing activities and the oil industry, in particular effects of seismic airgun sounds on fish behavior and fisheries. He has published 50 peer-reviewed papers based on his scientific research activities. During his two sabbaticals, he worked as a Visiting Scientist at Hatfield Marine Science Center, Newport, OR and at the Fishing Technology Service (FIIT), Fisheries Department of the Food and Agriculture Organization of the United Nations (FAO), Rome, Italy.

Dr. Løkkeborg is a member of the Acoustical Society of America (ASA) Standards Working Group on Effects of Sound on Fishes and Sea Turtles, the International Council for the Exploration of the Sea/Fisheries Department of the Food and Agriculture Organization of the United Nations (ICES-FAO) Working Group on Fishing Technology and Fish Behaviour, the Agreement on the Conservation of Albatrosses and Petrels (ACAP) Seabird Bycatch Working Group, and the Referral Group of Southern Seabird Solutions Trust.